Research Article | Vol. 27, No. 8 | 15 Apr 2019 | OPTICS EXPRESS 10482

Optics EXPRESS

Quantum critical detector: amplifying weak signals using discontinuous quantum phase transitions

LI-PING YANG[1] AND ZUBIN JACOB[1,*]

Birck Nanotechnology Center and Purdue Quantum Center, School of Electrical and Computer Engineering, Purdue University, West Lafayette, IN 47906, USA
[*]*zjacob@purdue.edu*
http://www.electrodynamics.org/

Abstract: We propose a quantum critical detector (QCD) to amplify weak input signals. Our detector exploits a first-order discontinuous quantum-phase-transition and exhibits giant sensitivity ($\chi \propto N^2$) when biased at the critical point. We propose a model consisting of spins with long-range interactions coupled to a bosonic mode to describe the time-dynamics in the QCD. We numerically demonstrate dynamical features of the first order (discontinuous) quantum phase transition such as time-dependent quantum gain in a system with 80 interacting spins. We also show the linear scaling with the spin number N in both the quantum gain and the corresponding signal-to-quantum noise ratio during the time evolution of the device. Our work shows that engineering first order discontinuous quantum phase transitions can lead to a device application for metrology, weak signal amplification, and single photon detection.

1. Introduction

Weak signal detection and amplification is a key process in metrology [1, 2], imaging [3], LIDAR [4], quantum communications and quantum computing [5]. There exist two widely used quantum amplification schemes for detecting weak signals. In the first kind, the weak input signal is directly amplified to generate a large output signal, as in quantum linear amplifiers [6–9]. It is widely utilized in circuit QED for parametric amplification in Josephson junction amplifiers [10]. Another scheme of amplification exists where the weak input perturbation functions as a control signal of an optimally biased device near the critical point. The practical realizations include single-electron transistors [11] and single-photon detectors [12]. This latter class can be classified as critically biased amplifiers. An important distinction of critically biased amplifiers from quantum linear amplifiers is that the input and output information carriers can be fundamentally different (eg: input photons and output electrons).

The amplification mechanism of a large class of weak signal detectors is based on thermodynamic (classical) phase transitions, which exhibits ultra-high sensitivity at the critical point, such as the superconducting single-photon detector [13] and the bubble chamber [14]. During the amplification, the incident weak signal triggers a phase transition of the critically biased detector to generate a large output signal. The goal of this paper is to propose a class of biased detectors with an amplification scheme that exploits quantum criticality in a first-order quantum phase transition (QPT). Our proposed device can be considered as an engineered quantum analog of widely utilized detectors which exploit naturally occurring thermodynamic phase transitions. We emphasize that the recent interest in engineering quantum phase transitions using qubit systems in ion traps [15], cold atoms [16] and circuit QED [17] forms an excellent platform to realize our proposed device. As QPTs happen at zero temperature, our proposed QCD may have higher signal-to-noise ratio and lower dark counting rate than detectors utilizing thermodynamic phase transitions.

A QPT at zero temperature describes an abrupt change in the ground state of a many-body

#358602 https://doi.org/10.1364/OE.27.010483
Journal © 2019 Received 24 Jan 2019; revised 17 Mar 2019; accepted 19 Mar 2019; published 1 Apr 2019

system [18, 19]. Most of the QPTs discovered in physical systems are of second-order [20–25] and they have also been proposed as a resource for metrology. However, no significant change in the number of excitations or energy transfer between subsystems occurs during a second-order QPT. To obtain an observable change in the output, a large parameter variation is required which can not be induced by a weak input signal (eg: single photon). Thus, high quantum gain can not be obtained using traditional second-order QPTs limiting their applicability for weak signal amplification. On the contrary, in a first-order (discontinuous) QPT, even a very small parameter variation at the critical point can lead to a significantly large change in the values of physical observables. Therefore, a universal model exhibiting first-order QPT with a well-understood microscopic mechanism can provide a natural platform for quantum amplification [6], quantum metrology [1, 2], and lead to new types of single-photon detectors.

We emphasize that time dynamics near the critical point fundamentally determines whether QPTs can be a practical resource for amplification and detection. Specifically, critical sensitivity in QPT results only from the transition between the ground states of two different phases but can not be realized by a unitary adiabatic evolution. Thus, a dynamical detection event which necessarily involves excited states of the detector may not connect these two ground states leading to completely sub-optimal critical behavior. Even though few first-order QPT models have already been found [26–29], the dynamics of these QPTs around the critical point have not been revealed. The application of these first-order QPTs is therefore an open problem, as practical detection events and amplifications are fundamentally dynamical processes. In this paper, we overcome this important challenge related to time dynamics near the quantum critical point and also present a fundamental advancement in the design of weak signal detectors.

We introduce a first-order QPT model, composed of a bosonic mode and a spin ensemble with long-range interaction. We numerically show that there exists a critical point in this system where the sensitivity χ diverges with N^2-scaling (N the spin number). This scaling is much faster than previous first-order phase transitions [30, 31] and provides extraordinary high sensitivity for weak signal detection. This first-order QPT and the giant sensitivity in our model fundamentally originate from the competition between two phases with long-range spin order. Exploiting this unique criticality, we propose a quantum critical detector (QCD) utilizing a weak input signal triggered first-order QPT [see the schematic in Fig. 1(a)]. We emphasize that the time-dynamics near a phase transition is a formidable challenge and we overcome this using the unique features of our proposed model. Via direct numerical evaluations, we demonstrate the time-dynamical features of a QCD consisting of 80 spins interacting with a bosonic mode. We show the existence of a first-order QPT in our QCD which sheds light on the microscopic origin of time-dependent quantum gain $g(t)$. Finally, we show the linear scaling in both the maximum quantum gain and the corresponding signal-to-quantum noise ratio (SQNR) during the time-evolution of our detector revealing high figures of merit. Our work motivates quantum devices with engineered discontinuous phase transitions for single photon detection.

2. Detection using discontinuous quantum phase transition

The key element of a QCD is the first-order QPT based quantum amplification. Here, we introduce a specific first-order QPT model composed of a bosonic mode and an interacting spin ensemble. The input to the device can be a weak signal (eg: single photon) which either perturbs the coupling between the bosonic mode and the spins or the couping between the individual spins. The output of the detector i.e. the amplified signal is the macroscopic population of the bosonic mode (see Fig. 1). The Hamiltonian of the system is given by

$$H = \hat{d}^{\dagger}\hat{d} + \frac{\lambda}{\sqrt{N}}\sum_{j=1}^{N}\hat{\sigma}_j^x(\hat{d}+\hat{d}^{\dagger}) + \frac{\epsilon}{2}\sum_{j=1}^{N}\hat{\sigma}_j^z - \frac{J}{N}\sum_{j<k}\hat{\sigma}_j^y\hat{\sigma}_k^y, \tag{1}$$

Optics EXPRESS

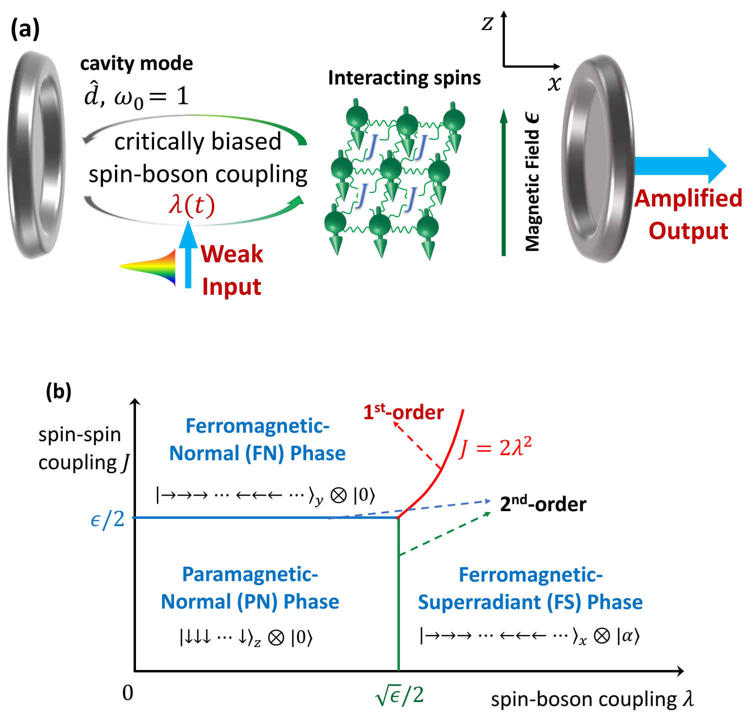

Fig. 1. (a) Schematic of the quantum critical detector (QCD). The bosonic mode (resonant cavity $\hat{d}$-mode) with frequency $\omega_0 = 1$ is the output mode. The spins are immersed in a homogeneous magnetic field along z-axis inducing an energy splitting ϵ. The spin-boson coupling λ is in x-direction and the all-to-all spin-spin coupling J is along y-axis. The input weak signal leads to a small time-dependent variation in spin-boson coupling $\lambda(t)$ and triggers a first-order quantum phase transition if the system is optimally biased around the critical point. The energy pre-stored in the spins transfers to the bosonic mode and realize the amplification in our QCD. (b) Phase diagram of our model and the schematic of the ground-state wave function of each phase. The green, blue, and red lines give the boundaries of the three quantum phases. In the strong-coupling regime $J > J_{c,\mathrm{II}} \equiv \epsilon/2$ and $\lambda > \lambda_{c,\mathrm{II}} \equiv \sqrt{\epsilon}/2$, the QPT between the FN phase and the FS phase (crossing the red line) is of first order. The other two QPTs are of second-order. Here, $|0\rangle$ and $|\alpha\rangle$ are the vacuum state and coherent state of the bosonic mode. The ground state of the spins in the ferromagnetic phase is a coherent spin state as explained in Appendix B.

Optics EXPRESS

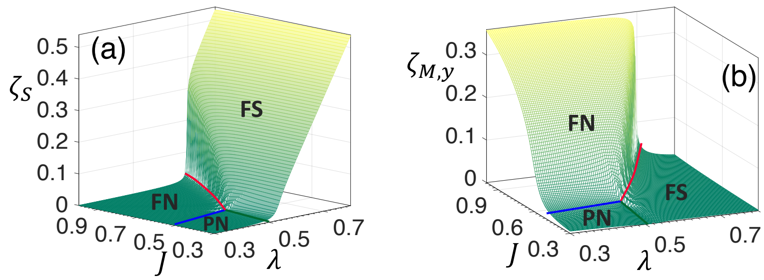

Fig. 2. Numerical demonstration of the phase diagram with the superradiant order parameter $\zeta_S = \langle \hat{d}^\dagger \hat{d} \rangle_0 / N$ in panel (a) and the magnetic order parameter $\zeta_{M,y} = \langle \hat{S}_y^2 \rangle_0 / N^2$ in panel (b). The boundaries between different phases are marked out by the blue, the green, and the red lines, which correspond to the three lines in Fig. 1(b) exactly. In this figure, the other parameters are taken as $\epsilon = 1$, and both the spin number N and the cutoff for the bosonic mode are set as 40.

Here, $\hat{d}(\hat{d}^\dagger)$ denotes the output bosonic mode. Its frequency has been taken as the unit of energy $\omega_0 = 1$ and all the other parameters in the Hamiltonian have been rescaled by ω_0. The operators $\hat{\sigma}_j^\alpha$ ($\alpha = x, y, z$) are the Pauli matrices of the jth spin. A magnetic field is applied along the z-direction inducing a energy splitting ϵ between spin states $|\uparrow\rangle_j$ and $|\downarrow\rangle_j$. The spin-boson coupling is along x-direction with homogeneous coupling strength λ similar to the Dicke model [32]. The last term describes the all-to-all homogeneous coupling between the spins along the y-direction akin to the Lipkin-Meshkov-Glick (LMG) model [21–23]. Here, we call this model as Dicke-LMGy model and emphasize the critical distinction from the Dicke-Ising model which only has nearest neighbour spin interactions [26]. The amplification process in the QCD is triggered by the weak input signal induced variation in the spin-boson coupling λ or equivalently the spin-spin coupling J.

To characterize the quantum phases and the corresponding QPTs in our Dicke-LMGy model, we introduce two new magnetic order parameters (OPs): $\zeta_{M,x} = \langle \hat{S}_x^2 \rangle_0 / N^2$ and $\zeta_{M,y} = \langle \hat{S}_y^2 \rangle_0 / N^2$ ($\hat{S}_\alpha = \sum_j \hat{\sigma}_j^\alpha / 2$ and $\langle \cdots \rangle_0$ means averaging on the ground state) characterizing the magnetic fluctuations in the spins along x and y axes, respectively. Such OPs can be probed experimentally through spin noise spectroscopy [33]. Note, we do not choose the traditional magnetic OP $M_z = \langle \hat{S}_z \rangle_0 / N$ [34], due to its incapability of characterizing the first-order QPT in our model [35]. The superradiant OP $\zeta_S = \langle \hat{d}^\dagger \hat{d} \rangle_0 / N$ is utilized to characterize the macroscopic excitation in the bosonic mode and functions as the output observable of our QCD. We emphasize that the fundamental competition between two ferromagnetic phases gives rise to a first order phase transition.

There exist three quantum phases in our model: paramagnetic-normal (PN) phase, ferromagnetic-normal (FN) phase, and ferromagnetic-superradiant (FS) phase as shown in Fig. 1(b) (more information about the quantum phases and ground-state wave functions can be obtained in Appendix A and B). In the λJ-plane, the the blue line determined by the critical spin-spin coupling strength $J_{c,\mathrm{II}} \equiv \epsilon/2$, the green line determined by the critical spin-boson coupling $\lambda_{c,\mathrm{II}} \equiv \sqrt{\epsilon}/2$, and the red line $J = 2\lambda^2$ give the phase boundaries. We emphasize that the FN-FS boundary displays a first order QPT which is necessary for our QCD. There exists a unique triple-point ($\lambda_{c,\mathrm{II}}$, $J_{c,\mathrm{II}}$) determined by the energy splitting ϵ. The numerical demonstration of the phase diagram is given in Fig. 2 with the superradiant OP ζ_S and the magnetic OP $\zeta_{M,y}$ in panels (a) and (b), respectively. The OP $\zeta_{M,x}$ not shown here behaves similarly to ζ_S. We exploit mean field theory [35, 36] to verify this phase diagram obtained by our direct numerical calculation. We emphasize that the numerical approach we have introduced holds a fundamental advantage for dynamical amplification and noise calculations.

Optics EXPRESS

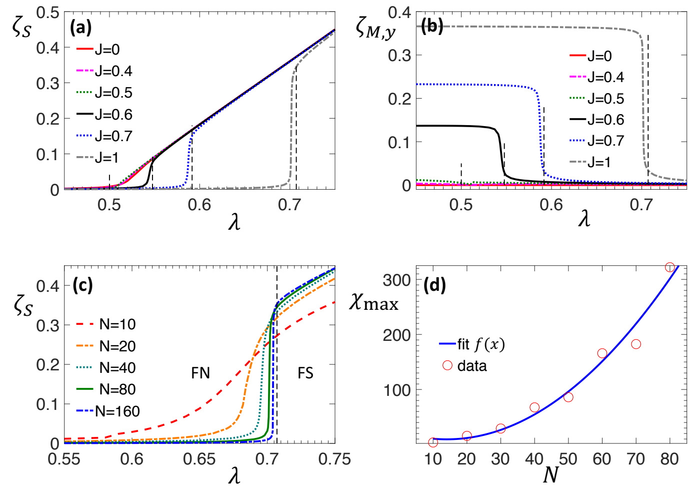

Fig. 3. In (a) and (b), we show the order parameters ζ_S and $\zeta_{M,y}$, respectively, for different spin-spin coupling J. Here, $\epsilon = 1$ and both the spin number and the cutoff of the bosonic mode are set as 80. Second-order QPTs occur at $\lambda_{c,\text{II}} \equiv \sqrt{\epsilon}/2 = 0.5$ for $J \leq J_{c,\text{II}} \equiv \epsilon/2 = 0.5$ and first-order QPTs occur at $\lambda_{c,\text{I}} \equiv \sqrt{J/2}$ for $J > J_{c,\text{II}}$. The locations of the critical points are marked by the thin black dashed line. In panel (c), we plot ζ_S with fixed $J = 1 > J_{c,\text{II}}$ for different spin number N. In panel (d), we show that the maximum of the sensitivity diverges with the spin number N verifying the first-order QPT. The polynomial fitting function $f(x) = 0.067x^2 - 1.881x + 22.62$ shows the N^2 scaling.

The most striking property of our tractable model is that the QPT between the FN phase and the ferromagnetic-superradiant (FS) phase is of first order making QCD a highly sensitive device. This first order transition occurs in the strong coupling regime for large spin-spin coupling ($J > J_{c,\text{II}}$) and spin-boson coupling ($\lambda > \lambda_{c,\text{II}}$). As shown by the black, blue, and gray lines in Fig. 3(a) and 3(b), discontinuous changes are observed in both the superradiant OP ζ_S and the magnetic OP $\zeta_{M,y}$. Note that the overlapping red, pink and green curves correspond to low spin-spin coupling giving rise only to a second order transition between the PN and FS phase, not suitable for QCD. Once the spin-spin coupling increases, there is no paramagnetic phase and there exists only a ferromagnetic phase for all spin-boson coupling strengths. This ferromagnetism is evident by studying the magnetic order parameter in Fig. 3(b) (black, blue and gray curves). We emphasize that the ferromagnetic behavior shown in Fig. 3(b) is only along the y direction and the exact opposite trend occurs for the x direction (not shown). During the FN to FS transition which is first order, the energy prestored in the spins transfers to the bosonic mode coupled with a change in the spin fluctuations from the y-direction to the x-direction. The first-order QPT results from the competition between the FS phase – that arises from strong spin-boson coupling along the x-axis and the FN phase – caused by large spin-spin coupling along the y-axis. We also predict that this type of first-order QPT should also exist in the Ising XY-model [27]. Another important characteristic is that the first-order phase transition point is sensitive to the spin-spin coupling (bias) while the second order ones in Fig. 2(a) is not.

We now explicitly show that the FN-FS phase transition is of first order in Fig. 3(c) as required for QCD. Increasing the spin number, the phase transition shows critical scaling behavior. Here, the sensitivity of the system at the critical point is determined by first-order derivative of the superradiant OP ζ_S,

$$\chi(\lambda) = \frac{1}{N}\frac{d}{d\lambda}\langle \hat{d}^\dagger \hat{d} \rangle, \tag{2}$$

Optics EXPRESS

where the factor $1/N$ is for consistency with the magnetic susceptibility. In Fig. 3(d), we plot the maximum of the sensitivity function ($\chi_{\max}$) at the first-order critical point $\lambda_{c,\mathrm{I}} \equiv \sqrt{J/2}$ vs spin number (N). In the thermodynamic limit $N \to \infty$, $\chi_{\max}$ diverges with speed $\propto N^2$, which is much faster than the $\sqrt{N}$-scaling obtained in the previous first-order dissipative transition [31] or the linear N scaling in the first-order thermodynamic phase transition predicted by Imry [37]. There are two main reasons resulting in the sensitivity differences between our device and the one using a thermodynamic phase transition of the Dicke-Ising model in Ref. [30]. First, we use the first-order QPT at zero temperature instead of a first-order thermodynamic phase transition at a finite temperature as in [30].]. Second, the $1/N^2$-scaling in sensitivity is obtained for small parameter variation at the critical point in the QPT. This is different from the $1/N$ scaling in sensing the temperature changing in [30]. We predict that higher sensitivity on the estimation of system parameters, especially the coupling strength (i.e., the spin-boson coupling λ or the spin-spin coupling J), can also be obtained via utilizing the first-order QPT in the Dicke-Ising model. This N^2 scaling, arising from competing phases, may be used to enhance the sensitivity in quantum metrology [38].

3. Dynamical quantum amplification

To utilize quantum criticality as a resource of quantum amplification, one has to study the dynamical behavior around the critical point. The challenge in exploiting QPTs for quantum amplification arises fundamentally from the fact that ground states of two different phases can not be connected via an adiabatic operation [39], as the gap of the system vanishes at the critical point in the thermodynamic limit. For example, starting from the ground state of the FN phase, the system can alternatively evolve to an arbitrary excited state instead of going to the ground state of the FS phase thereby completely negating critical amplification. To demonstrate the dynamical nonlinear amplification, here we show the dynamics of the first-order QPT in our model with 80 spins via direct numerical time-evolution. A QCD is demonstrated with the large quantum gain around the critical point after a QPT triggered by a time-varying parameter. We also show that a linear scaling with the spin number N in the quantum gain and SQNR of the QCD is obtained, instead of the N^2 in the sensitivity of the first-order QPT.

The full measurement in our QCD is split into two main processes: transduction (absorption) and amplification. After the transduction, the excitations or energy in the input signal will be transferred into the detector. We model this process by considering a temporal variation in the spin-boson coupling. A physical mechanism for this process can be the radiation pressure of the photon falling on the walls of a cavity. An equivalent model can be a temporal variation in the spin-spin coupling. We note that time-dependent theory of phase transitions as well as single photon interaction with a system biased near a phase transition is an open challenge. To overcome this, we use the following approach to simulate the time dynamics in our system. We fix the trajectory of a parameter in the Hamiltonian and directly evaluate the time-dependent dynamics of the spins as well as the bosonic mode. This is numerically tractable due to the reduced Hilbert space in a system with all-to-all spin coupling.

To depict the weak signal interaction with our detector, we introduce a time-dependent variation of the spin-boson coupling strength $\lambda(t) = \lambda_0 + \Delta\lambda \times P_e(t)$ and solve the entire time dynamics near the first order phase transition. The key amplification process in our QCD occurs from first-order QPT process triggered by this time-dependent parameter $\lambda(t)$. The spin-boson coupling λ_0 is optimally tuned to be very close to the critical point $\lambda_{c,\mathrm{I}}$ and the detector is prepared on the ground state of the system, which functions as the "quantum" bias. Thus, even a very small parameter variation $\Delta\lambda$ (amplitude) can trigger a QPT and leads to efficient amplification. As mentioned before, amplification is defined as the enhanced number of bosons in the cavity mode. The time-dependent envelope $P_e(t)$ of the coupling $\lambda(t)$ is determined by the transduction process. One example of such a weak input signal is a single-photon. The absorption process

Optics EXPRESS

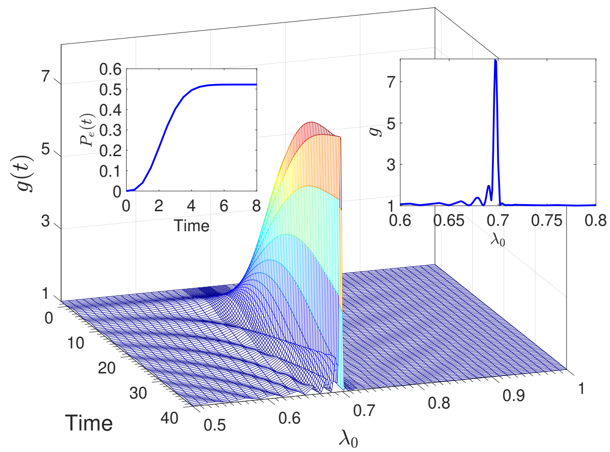

Fig. 4. The amplification via the first-order dynamical quantum phase transition is shown by the time-dependent quantum gain $g(t)$. The left subplot shows envelope $P_e(t)$ in the time dependent spin-boson coupling $\lambda(t)$. Here, the spin-spin coupling is set as $J = 1 > J_{c,\mathrm{II}}$, the time is in a unit of $1/\omega_0$, and amplitude of the small change in the parameter $\lambda(t)$ is set to be $\Delta\lambda = 0.01$. In the right subplot, we show that the quantum amplification only occurs when λ_0 is biased close to critical point $\lambda_{c,\mathrm{I}} = \sqrt{J/2} \approx 0.707$ with $t = 40$.

is probabilistic [40] and results in a wave form of the quantum excitation in a detector (more information about $P_e(t)$ can be found in Appendix C). The full dynamics of the whole system is governed by the time-dependent Hamiltonian $H(t)$ in Eq. (1) by replacing λ with $\lambda(t)$. To characterize the detection sensitivity, we define the quantum gain of the amplification in our QCD as

$$g(t) = \langle \hat{d}^\dagger(t)\hat{d}(t)\rangle / \langle \hat{d}^\dagger(0)\hat{d}(0)\rangle, \tag{3}$$

where $\langle \hat{d}^\dagger(t)\hat{d}(t)\rangle$ is the mean value of the time-dependent operator in the Heisenberg picture on the ground state of initial Hamiltonian $H(0)$ with $\lambda = \lambda_0$.

The dynamical amplification in the QCD is demonstrated by the time-dependent gain as a function of the bias spin-boson coupling λ_0 and time in Fig. 4. We see that the efficient amplification can only be obtained if the system is optimally biased close to the critical point. In the right subplot computed at fixed time $t = 40$, we explicitly show the high gain of our QCD around the critical point. Here, we show the highly sensitive nature of a time-dependent first-order QPT system to the initial bias. Similar to the enhanced decay of the Loschmidt echo by the criticality in a second-order QPT [19], the enhanced quantum gain in our QCD is a universal characteristic of criticality in a first-order QPT, which can be tested in experiments.

To show the high figures of merit of our QCD, we present the scaling of the quantum amplification with the spin number N in Fig. 5. The maximum gain is shown to be linearly proportional to N. This result should be contrasted with the amplification resulting from the second order phase transition with $J \le J_{c,\mathrm{II}}$ (see pink triangle line and the green circle line). The latter is much smaller than the one from the first-order QPT with $J > J_{c,\mathrm{II}}$ (see the blue diamond line). In the right subplot, we show the slope of $g_{\max}$ with the spin number for different spin-spin coupling. There exists a "phase transition" phenomenon in the slope at the same critical point $J_{c,\mathrm{II}}$ of the transition from second-order to first-order QPTs. To characterize the quantum noise in our QCD, we define the SQNR as [41]

$$\mathrm{SQNR} = \langle \hat{d}^\dagger(t)\hat{d}(t)\rangle^2 / \langle [\Delta\hat{d}^\dagger(t)\hat{d}(t)]^2\rangle, \tag{4}$$

where $\langle [\Delta\hat{d}^\dagger(t)\hat{d}(t)]^2\rangle = \langle [\hat{d}^\dagger(t)\hat{d}(t)]^2\rangle - \langle \hat{d}^\dagger(t)\hat{d}(t)\rangle^2$ is the variance of the bosonic excitation

Optics EXPRESS

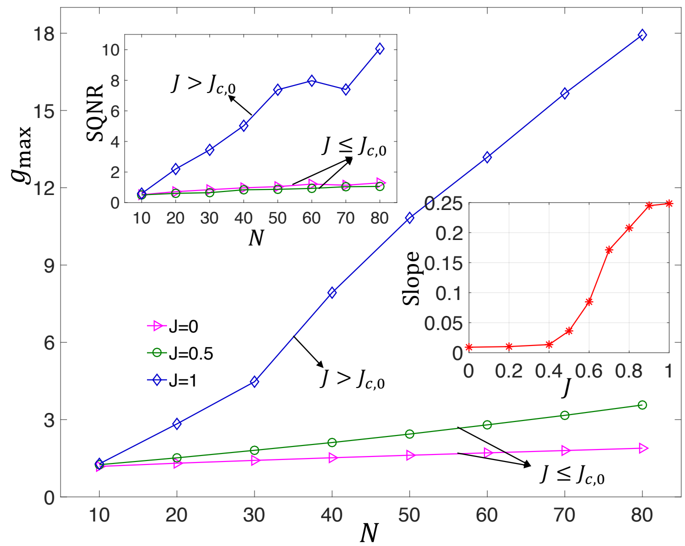

Fig. 5. Linear scaling of the quantum bosonic amplification with the spin number N for different spin-spin coupling J. The corresponding signal-to-quantum noise ratios are shown in the left subplot. In the right subplot, we shown there is a phase-transition-like behavior in the slope of the maximum gain when J crosses the critical point $J_{c,\text{II}} = 0.5$. First-order dynamic QPT (blue diamond line) has much higher gain and signal-to-quantum noise ratio than that of second-order QPT.

number operator. The corresponding SQNR for the three lines are displayed in the left subplot. It shows amplification based on first-order QPT has much higher SQNR than that of second-order QPTs. Similar to the quantum gain (the re-scaled excitation number in the output bosonic mode), the SQNR also increases linearly with the spin number, which is consistent with the SQNR of a coherent state as the final output state. Our proposed detector exploits quantum criticality of interacting spins for amplification. Hence, it is necessary for the amplification time and phase transition to complete before the decoherence of spins occurs. This is possible in principle as evidenced by recent demonstrations of quantum phase transitions in engineered ion trap [15], Rydberg atom [16], and circuit QED [17] systems.

4. Conclusion

We have proposed to engineer first-order (discontinuous) QPTs for weak-signal detection. Our proposed device is a quantum analog of widely used detectors which exploit thermodynamic phase transitions. One of the key differences between the thermodynamic and quantum phase transition based detectors is that the thermodynamic process requires the weak signal to change the temperature of the macroscopic system. In contrast, the quantum phase transition can work at constant low temperature and the weak signal can couple to other parameters/dynamical degrees of freedom in the system. As an example, we explicitly demonstrated the dynamical amplification by utilizing the high-sensitivity at the first-order critical point in the Dicke-LMG model we introduced. In recent experiments, second-order QPTs have been demonstrated with Bose-Einstein condensates [42], trapped ions [15], cold atoms [16], and superconducting qubits [17]. However, the quantum critical detector requires engineered first order phase transitions which is still an open challenge. We believe these platforms provide a starting point for physical realization of our proposed device where single photon perturbations can trigger a phase transition in systems with long-range interactions. Our work also motivates large scale macroscopic modeling of

Optics EXPRESS

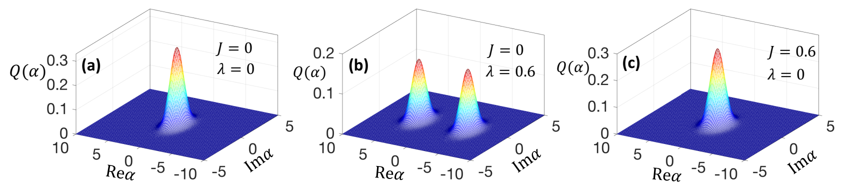

Fig. 6. The Husimi Q-functions of the bosonic mode on the ground states of the paramagnetic-normal phase (a), the ferromagnetic-superradiant phase (b), and the ferromagnetic-normal phase (c) are displayed. Here, the other parameters are set as $\epsilon = 1$, spin number $N = 80$, and the bosonic mode cutoff 80.

devices with a single quantum of energy propagating through it.

A. Defining quantum phases in the detector

By defining the collective angular momentum operators of the N spins

$$\hat{S}_\alpha = \frac{1}{2}\sum_{j=1}^{N}\hat{\sigma}_j^\alpha, \ \alpha = x, y, z, \tag{5}$$

we can rewrite our model Hamiltonian as

$$H = \hat{d}^\dagger\hat{d} + \frac{2\lambda}{\sqrt{N}}\hat{S}_x(\hat{d} + \hat{d}^\dagger) + \epsilon\hat{S}_z - \frac{2J}{N}\hat{S}_y^2. \tag{6}$$

One can see that the spin ensemble is equivalent to a single particle with spin-$N/2$ [43]. As the total angular momentum of the spin ensemble is conserved, we can perform the numerical simulation within a subspace spanned by the $N + 1$ Dicke states [32]. This makes our model become tractable in numerical simulation.

There exist three quantum phases in our model: paramagnetic-normal (PN) phase, ferromagnetic-normal (FN) phase, and ferromagnetic-superradiant (FS) phase. The phase diagram of our model can be obtained via direct numerical evaluation. By exploiting a mean-field theory [36], we verify our numerical simulation and also obtain the exact analytical wave function of the ground states [35].

B. Ground-state wave function of the detector

To reveal the underlying microscopic mechanism of our quantum critical detector (QCD), we need to understand the fundamental changes in the ground state of the system during the quantum phase transitions (QPTs). As we known, the Husimi Q-function is a quantum analog of the classical distribution function in the phase space, which provide a powerful tool to vividly show the ground-state wave function of the system in each phase.

The bosonic Husimi Q is defined as [44],

$$Q(\alpha) = \frac{1}{\pi}\mathrm{Tr}_{\mathrm{spin}}[\langle\alpha|\rho_{\mathrm{g}}|\alpha\rangle], \tag{7}$$

where ρ_g is the density matrix of the ground state, $|\alpha\rangle$ is an arbitrary bosonic coherent state, and $\mathrm{Tr}_{\mathrm{spin}}[\cdots]$ means tracing off the degrees of freedom of the spins. For the spin degree of freedom, the Bloch sphere is usually utilized to characterize an arbitrary state of spin-1/2 particle. But for a spin-n particle, a $[(2n+1)^2 - 1]$-dimensional sphere is required. It is impossible to show such a high-dimensional sphere. To overcome this issue, we introduce the spin Husimi Q-function [45],

$$Q(\theta, \phi) = \frac{2N+1}{4\pi}\mathrm{Tr}_{\mathrm{boson}}[\langle\theta, \phi|\,\rho_{\mathrm{g}}\,|\theta, \phi\rangle], \tag{8}$$

Optics EXPRESS

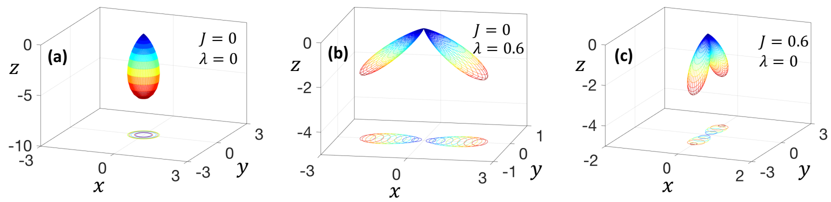

Fig. 7. The Husimi Q-functions of the spins for the ground states ρ_g of the paramagnetic-normal phase (a), the ferromagnetic-superradiant phase (b), and the ferromagnetic-normal phase (c) are displayed. Here, the spherical coordinates ($r = Q(\theta, \phi), \theta, \phi$) have been transferred to the corresponding Cartesian coordinates (x, y, z). The curves underneath are the contour projections of the corresponding Q-functions in xy-plane. The other parameters are set as $\epsilon = 1$, spin number $N = 80$, and the bosonic mode cutoff 80.

where N is the spin number, $\mathrm{Tr}_{\mathrm{boson}}[\cdots]$ means tracing off the degrees of freedom of the bosonic mode, and $|\theta, \phi\rangle$ is a coherent spin state [46, 47]. To let the angle θ be the exact same polar angle of a spherical coordinate, we redefine the coherent spin state as,

$$|\theta, \phi\rangle = e^{i\theta(\hat{S}_x \sin\phi - \hat{S}_y \cos\phi)} |N/2, N/2\rangle . \tag{9}$$

Here, $|N/2, N/2\rangle$ is the Dicke state with all the spins on the up state.

Our numerical approach allows us to directly calculate the ground states and the corresponding Husimi Q-functions of the system. In the paramagnetic-normal (PN) phase, the bosonic mode is on the vacuum state. As shown in Fig. 6(a), the bosonic Q-function has only one peak located at the origin. In this phase, the spins are on the Dicke state $|N/2, -N/2\rangle$, i.e., all the spins are polarized along negative z-axis. As shown in Fig. 7(a), the corresponding spin Q-function is a cigar-like structure lying along negative z-axis. From this quasi-probability distribution function, we can see that the mean magnetization $M_z = \langle \hat{S}_z \rangle_0 / N$ ($\langle \cdots \rangle_0$ means averaging on the ground state) is a finite negative value, but the two magnetic order parameters $\zeta_{M,x} = \langle \hat{S}_x^2 \rangle_0 / N^2$ and $\zeta_{M,y} = \langle \hat{S}_y^2 \rangle_0 / N^2$ are very small and will go to zero in the limit $N \longrightarrow \infty$.

The ferromagnetic-superradiant (FS) phase has two degenerate ground states $|\alpha_0\rangle \otimes |\theta_0, \pi\rangle$ and $|-\alpha_0\rangle \otimes |\theta_0, 0\rangle$. Here, $|\alpha_0\rangle$ is a bosonic coherent state and $|\theta_0, \phi_0\rangle$ ($\phi_0 = 0,\ \pi$) is a coherent spin state. The value of α_0 and θ_0 can be determined by the mean-field theory in the thermodynamic limit $N \longrightarrow \infty$ [35]. When the system adiabatically goes to the FS phase, the system can be on an arbitrary superposition of these two degenerate states. Thus, the ensemble mean value of the displacement of the bosonic mode $\langle \hat{d}^\dagger + \hat{d} \rangle_0$, the magnetization along x-direction $\langle \hat{S}_x \rangle_0$, and the magnetization along y-direction $\langle \hat{S}_y \rangle_0$ are all zero. But the excitation number reflected in the superradiant order parameter $\zeta_S = \langle \hat{d}^\dagger \hat{d} \rangle_0 / N$ and the magnetic noise characterized by the magnetic order parameter $\zeta_{M,x}$ are finite. In the numerical simulation, we choose the ground state as a symmetric superposition of these two degenerate states. In Fig. 6(b), we show the Q-function of the bosonic mode. The two separated peaks on the real axis indicate the macroscopic excitation in the bosonic mode. In Fig. 7(b), we also see the rotation of the spins in the xz-plane as the strong spin-boson coupling λ is along x-axis. These two branches correspond to the two degenerate states.

The ferromagnetic-normal (FN) phase also has two degenerate states $|0\rangle \otimes |\theta_0, \pi/2\rangle$ and $|0\rangle \otimes |\theta_0, 3\pi/2\rangle$. When the system adiabatically goes to the FN phase, the bosonic mode is always on the vacuum state as shown by the corresponding Q-function in Fig. 6(c). But the spins can be on an arbitrary superposition of these two coherent spin states $|\theta_0, \phi_0\rangle$ ($\phi_0 = \pi/2,\ 3\pi/3$). Thus, the ensemble mean of the magnetization in xy-plane is still zero. But the magnetic noise characterized by the magnetic order parameter $\zeta_{M,x}$ is finite. The Q-function of the spin in the FN phase is displayed in Fig. 7(c). The strong spin-spin coupling J along y-axis leads to the

Optics EXPRESS

rotation of the spins in yz-plane. Here, we can also see that, when QPT from the FN phase to the FS phase occurs, the energy prestored in the spins transfers to the bosonic mode contributing to the macroscopic excitation in the bosonic mode. Also, a fundamental change in the spin noise from the y-direction to the x-direction can be observed.

The QPTs of PN↔FN and PN↔FS are of second order. Only the transition FN↔FS is a first order one. We emphasize that second order phase transitions which are continuous phase transitions do not possess the necessary features for quantum critical detection. In stark contrast, first order discontinuous phase transitions exhibit a giant response when a weak perturbation is applied making them an ideal resource for quantum critical detection.

C. Analogy with practical single-photon detectors

To clearly explain the motivation of our work, we show the analogy of our proposed detector with the practical single-photon detectors. As we mentioned in the main text, there are two main amplification schemes: quantum linear amplifiers and critically biased amplifiers. We are focusing on the second amplification scheme, where the weak input signal does not get amplified directly. Instead, it functions as a control of an optimally biased critical system, which is significantly different from the first one, such as quantum linear amplifiers. In these critically biased amplifiers, the input and output information carriers can be fundamentally different (eg: input photons and output electrons) and the corresponding gain is defined as the ratio of the outputs with and without the input control signal. In this section, we show the analogy of our proposed QCD with the practical critical detectors to explain the motivation of our work more clearly. Finally, we show that first-order QPT-based devices can pave a way for new types of weak signal detector.

We first take the superconducting nanowire single-photon detector (SSNPD) as an example to explain the critical amplification scheme explicitly. The SSNPD is the best available and widely used near-infrared single-photon detector with $\geq 95\%$ quantum efficiency [48], < 3 picoseconds timing jitter [49] and < 1 dark count per hour [50]. The input is a single-photon pulse—an extremely weak quantum signal. The current in the superconducting nanowire is biased very close to the critical current, thus even a single-photon pulse can break the superconductivity. The output signal is the voltage difference between the two ends of the superconducting nanowire. In the transduction (absorption) process, the incident single-photon pulse will general one resonantly excited electron. As the center frequency of the pulse is much larger than the energy gap of the superconductor, this highly excited electron will break hundreds of Cooper pairs, reduce the local density of the superconducting electrons, and finally triggers a phase transition from a superconductor to a normal metal. Before the absorption of the photon, the voltage difference is extremely small. After the absorption of the photon, the superconducting nanowire becomes a normal metal. An observable output voltage pulse will be generated to realize the amplification. The amplification process in the SNSPD can be modeled as a time-varying local temperature induced thermodynamic phase transition. Similarly, we describe the amplification process of our QCD as the time-dependent system parameter variation induced first-order QPT. During the amplification process, the exact dynamical change in the superconducting electron density and the effective time-dependent local temperature can be obtained by numerical simulation.

This type of critically biased amplifiers has been extensively used in practical measurements even outside the context of SNSPDs, like the photomultiplier tube, the single-photon avalanche diode, single-electron transistor, etc. However, our proposed QCD is the first quantum analog of the classical critical detectors. Similarly, we also need to bias the detector very close to the critical point. After the absorption of the input weak signal, a time-dependent variation in the system parameter (such as the spin-boson coupling or spin-spin interaction strength) is induced to trigger a first-order dynamical QPT. For a specific measurement process, we also need to calculate the exact form of time-dependent change in system parameters. Without loss of generality, we

Optics EXPRESS

assume the time-varying spin-boson coupling change is proportional to the signal absorption probability $P_e(t)$ as shown in the subplot of Fig. 4 in the main text. The absorption probability $P_e(t)$ can be obtained by calculating the master equation of a quantized time-dependent pulse interacting with a quantum system as shown in [40, 51]. We show that, if the QCD is biased close to the critical point, a large amplification factor (the quantum gain) can be obtained.

During the dynamical amplification, the system parameter (coupling strength) is varied across the phase boundary time-dependently by the incident pulse. It is widely debated and is an open question whether QPTs retain their criticality during a dynamical process. The discontinuous change of the observable and the N^2 sensitivity found in the first-order QPT only occurs if the system goes from the ground state in one phase to the ground state of another phase. However, in a dynamical process, the system will not go to the ground state of the other phase but evolves to some complicated excited state. Therefore, we numerically studied the dynamics of the system around the critical point. We showed for the first time that the high sensitivity also exists in a dynamical process and thus explicitly demonstrated the dynamical amplification.

Funding

DARPA DETECT ARO award (W911NF-18-1-0074).

References

1. V. Giovannetti, S. Lloyd, and L. Maccone, "Quantum-enhanced measurements: beating the standard quantum limit," Science **306**, 1330–1336 (2004).
2. V. Giovannetti, S. Lloyd, and L. Maccone, "Quantum metrology," Phys. Rev. Lett. **96**, 010401 (2006).
3. L. Lugiato, A. Gatti, and E. Brambilla, "Quantum imaging," J. Opt. B: Quantum semiclassical optics **4**, S176 (2002).
4. A. Swatantran, H. Tang, T. Barrett, P. DeCola, and R. Dubayah, "Rapid, high-resolution forest structure and terrain mapping over large areas using single photon lidar," Sci. Reports **6**, 28277 (2016).
5. M. A. Nielsen and I. Chuang, "Quantum computation and quantum information," (2002).
6. C. M. Caves, "Quantum limits on noise in linear amplifiers," Phys. Rev. D **26**, 1817 (1982).
7. W. H. Louisell, A. Yariv, and A. E. Siegman, "Quantum fluctuations and noise in parametric processes. I.," Phys. Rev. **124**, 1646–1654 (1961).
8. B. R. Mollow and R. J. Glauber, "Quantum theory of parametric amplification. i," Phys. Rev. **160**, 1076–1096 (1967).
9. U. Gavish, B. Yurke, and Y. Imry, "Generalized constraints on quantum amplification," Phys. Rev. Lett. **93**, 250601 (2004).
10. A. Roy and M. Devoret, "Introduction to parametric amplification of quantum signals with josephson circuits," Comptes Rendus Physique **17**, 740–755 (2016).
11. M. H. Devoret and R. J. Schoelkopf, "Amplifying quantum signals with the single-electron transistor," Nature **406**, 1039 (2000).
12. M. Eisaman, J. Fan, A. Migdall, and S. V. Polyakov, "Invited review article: Single-photon sources and detectors," Rev. scientific instruments **82**, 071101 (2011).
13. G. GolâĂŹTsman, O. Okunev, G. Chulkova, A. Lipatov, A. Semenov, K. Smirnov, B. Voronov, A. Dzardanov, C. Williams, and R. Sobolewski, "Picosecond superconducting single-photon optical detector," Appl. Phys. Lett. **79**, 705–707 (2001).
14. D. A. Glaser, "Some effects of ionizing radiation on the formation of bubbles in liquids," Phys. Rev. **87**, 665 (1952).
15. J. Zhang, G. Pagano, P. W. Hess, A. Kyprianidis, P. Becker, H. Kaplan, A. V. Gorshkov, Z.-X. Gong, and C. Monroe, "Observation of a many-body dynamical phase transition with a 53-qubit quantum simulator," Nature **551**, 601 (2017).
16. H. Bernien, S. Schwartz, A. Keesling, H. Levine, A. Omran, H. Pichler, S. Choi, A. S. Zibrov, M. Endres, M. Greiner *et al.*, "Probing many-body dynamics on a 51-atom quantum simulator," Nature **551**, 579 (2017).
17. R. Harris, Y. Sato, A. J. Berkley, M. Reis, F. Altomare, M. H. Amin, K. Boothby, P. Bunyk, C. Deng, C. Enderud, S. Huang, E. Hoskinson, M. W. Johnson, E. Ladizinsky, N. Ladizinsky, T. Lanting, R. Li, T. Medina, R. Molavi, R. Neufeld, T. Oh, I. Pavlov, I. Perminov, G. Poulin-Lamarre, C. Rich, A. Smirnov, L. Swenson, N. Tsai, M. Volkmann, J. Whittaker, and J. Yao, "Phase transitions in a programmable quantum spin glass simulator," Science **361**, 162–165 (2018).
18. S. Sachdev, *Quantum phase transitions* (Wiley Online Library, 2007).
19. H. T. Quan, Z. Song, X. F. Liu, P. Zanardi, and C. P. Sun, "Decay of loschmidt echo enhanced by quantum criticality," Phys. Rev. Lett. **96**, 140604 (2006).
20. E. Lieb, T. Schultz, and D. Mattis, "Two soluble models of an antiferromagnetic chain," Annals Phys. **16**, 407–466 (1961).
21. H. J. Lipkin, N. Meshkov, and A. Glick, "Validity of many-body approximation methods for a solvable model:(i). exact solutions and perturbation theory," Nucl. Phys. **62**, 188–198 (1965).

Optics EXPRESS

22. N. Meshkov, A. Glick, and H. Lipkin, “Validity of many-body approximation methods for a solvable model:(ii). linearization procedures,” Nucl. Phys. **62**, 199–210 (1965).
23. A. Glick, H. Lipkin, and N. Meshkov, “Validity of many-body approximation methods for a solvable model:(iii). diagram summations,” Nucl. Phys. **62**, 211–224 (1965).
24. K. Hepp and E. H. Lieb, “On the superradiant phase transition for molecules in a quantized radiation field: the dicke maser model,” Annals Phys. **76**, 360–404 (1973).
25. Y. K. Wang and F. Hioe, “Phase transition in the dicke model of superradiance,” Phys. Rev. A **7**, 831 (1973).
26. C. F. Lee and N. F. Johnson, “First-order superradiant phase transitions in a multiqubit cavity system,” Phys. review letters **93**, 083001 (2004).
27. A. A. Ovchinnikov, D. V. Dmitriev, V. Y. Krivnov, and V. O. Cheranovskii, “Antiferromagnetic ising chain in a mixed transverse and longitudinal magnetic field,” Phys. Rev. B **68**, 214406 (2003).
28. J. Vidal, R. Mosseri, and J. Dukelsky, “Entanglement in a first-order quantum phase transition,” Phys. Rev. A **69**, 054101 (2004).
29. L. Del Re, M. Fabrizio, and E. Tosatti, “Nonequilibrium and nonhomogeneous phenomena around a first-order quantum phase transition,” Phys. Rev. B **93**, 125131 (2016).
30. S. Gammelmark and K. Mølmer, “Phase transitions and heisenberg limited metrology in an ising chain interacting with a single-mode cavity field,” New J. Phys. **13**, 053035 (2011).
31. M. Raghunandan, J. Wrachtrup, and H. Weimer, “High-density quantum sensing with dissipative first order transitions,” Phys. Rev. Lett. **120**, 150501 (2018).
32. R. H. Dicke, “Coherence in spontaneous radiation processes,” Phys. Rev. **93**, 99 (1954).
33. V. S. Zapasskii, “Spin-noise spectroscopy: from proof of principle to applications,” Adv. Opt. Photonics **5**, 131–168 (2013).
34. P. Pfeuty, “The one-dimensional ising model with a transverse field,” ANNALS Phys. **57**, 79–90 (1970).
35. L.-P. Yang and Z. Jacob, *Engineering Quantum Phase Transitions for Weak Signal Detection* (2018). Under preparation.
36. Y. Zhang, L. Yu, J.-Q. Liang, G. Chen, S. Jia, and F. Nori, “Quantum phases in circuit qed with a superconducting qubit array,” Sci. reports **4**, 4083 (2014).
37. Y. Imry, “Finite-size rounding of a first-order phase transition,” Phys. Rev. B **21**, 2042 (1980).
38. M. Skotiniotis, P. Sekatski, and W. Dür, “Quantum metrology for the ising hamiltonian with transverse magnetic field,” New J. Phys. **17**, 073032 (2015).
39. J. Dziarmaga, “Dynamics of a quantum phase transition and relaxation to a steady state,” Adv. Phys. **59**, 1063–1189 (2010).
40. L.-P. Yang, H. X. Tang, and Z. Jacob, “Concept of quantum timing jitter and non-markovian limits in single-photon detection,” Phys. Rev. A **97**, 013833 (2018).
41. H. Yuen, “States that give the maximum signal-to-quantum noise ratio for a fixed energy,” Phys. Lett. A **56**, 105–106 (1976).
42. K. Baumann, C. Guerlin, F. Brennecke, and T. Esslinger, “Dicke quantum phase transition with a superfluid gas in an optical cavity,” Nature **464**, 1301 (2010).
43. L.-P. Yang, Y. Li, and C. Sun, “Franck-condon effect in central spin system,” The Eur. Phys. J. D **66**, 300 (2012).
44. K. Husimi, “Some formal properties of the density matrix,” Proc. Physico-Mathematical Soc. Jpn. 3rd Ser. **22**, 264–314 (1940).
45. C. T. Lee, “q representation of the atomic coherent states and the origin of fluctuations in superfluorescence,” Phys. Rev. A **30**, 3308–3310 (1984).
46. J. Radcliffe, “Some properties of coherent spin states,” J. Phys. A: Gen. Phys. **4**, 313 (1971).
47. F. Arecchi, E. Courtens, R. Gilmore, and H. Thomas, “Atomic coherent states in quantum optics,” Phys. Rev. A **6**, 2211 (1972).
48. A. E. Lita, A. J. Miller, and S. W. Nam, “Counting near-infrared single-photons with 95% efficiency,” Opt. Express **16**, 3032–3040 (2008).
49. B. Korzh, Q. Zhao, S. Frasca, J. Allmaras, T. Autry, E. Bersin, M. Colangelo, G. Crouch, A. Dane, T. Gerrits *et al.*, “Demonstrating sub-3 ps temporal resolution in a superconducting nanowire single-photon detector,” arXiv preprint arXiv:1804.06839 (2018).
50. C. Schuck, W. H. Pernice, and H. X. Tang, “Waveguide integrated low noise nbtin nanowire single-photon detectors with milli-hz dark count rate,” Sci. Reports **3**, 1893 (2013).
51. B. Q. Baragiola, R. L. Cook, A. M. Brańczyk, and J. Combes, “N-photon wave packets interacting with an arbitrary quantum system,” Phys. Rev. A **86**, 013811 (2012).